LETTERS

Force production by disassembling microtubules

Ekaterina L. Grishchuk[1,2], Maxim I. Molodtsov[1,3], Fazly I. Ataullakhanov[3,4,5] & J. Richard McIntosh[1]

Microtubules (MTs) are important components of the eukaryotic cytoskeleton: they contribute to cell shape and movement, as well as to the motions of organelles including mitotic chromosomes. MTs bind motor enzymes that drive many such movements, but MT dynamics can also contribute to organelle motility[1–8]. Each MT polymer is a store of chemical energy that can be used to do mechanical work, but how this energy is converted to motility remains unknown. Here we show, by conjugating glass microbeads to tubulin polymers through strong inert linkages, such as biotin–avidin, that depolymerizing MTs exert a brief tug on the beads, as measured with laser tweezers. Analysis of these interactions with a molecular-mechanical model of MT structure and force production[9,10] shows that a single depolymerizing MT can generate about ten times the force that is developed by a motor enzyme; thus, this mechanism might be the primary driving force for chromosome motion. Because even the simple coupler used here slows MT disassembly, physiological couplers may modulate MT dynamics *in vivo*.

It has previously been proposed that MTs might generate force through their unusual mechano-chemistry[5,10]. These polymers assemble from tubulin dimers that bind GTP and hydrolyse it after polymerization. The GDP-bound dimer conformation is bent relative to its GTP-bound counterpart[11,12], but this bend is constrained by MT geometry so that some energy from GTP hydrolysis is stored in the polymer lattice[13,14]. During depolymerization, the accumulated stress forces the strands of GDP-bound dimers, or 'protofilaments' (PFs), to arch out in a 'ram's horn' configuration[15]. Thus, each MT is a reservoir of chemical energy that can be harnessed to do mechanical work. Two aspects of this mechanism have gone uncharacterized: the power-stroke, which is probably generated by curving PFs; and the coupling devices that might convert this energy into motility. Here we have conjugated glass microbeads to MTs and used laser tweezers to measure the forces exerted on the beads as the MTs depolymerize.

Biotinylated MTs were grown from *Tetrahymena* 'pellicles' (that is, lysed, de-ciliated protozoa), which will bind to the coverslip that tops a microscope chamber. Such pellicles define the orientation of the MTs that grow from them (the fast-growing or 'plus' ends are distal), and they provide a firm anchorage for the minus ends[6] (Fig. 1a). These labile MTs were capped with rhodamine-conjugated tubulin without biotin by extending existing polymers in the presence of GMPCPP, a slowly hydrolysable GTP analogue that forms stable MTs[16]. Glass microbeads coated with streptavidin were then allowed to bind to the biotinylated MT segments (Fig. 1b). To begin an experiment, the stable, rhodamine-labelled MT caps were dispersed by green light, which excites rhodamine fluorescence and induces the caps to break up[17]. The labile segments of the MTs were then exposed and depolymerized from their plus ends.

As the MTs depolymerized, the bound beads were released. We used laser tweezers to investigate the accompanying mechanical transients. Before a typical experiment our tweezers pulled an MT-attached bead toward the plus end of the polymer with an average of 0.5 pN. The position of the bead relative to the centre of the trap was measured with the much weaker beam from a tracking laser, imaged on a quadrant photodiode (QPD)[18,19] (Fig. 2). Non-random bead motions were usually detected within 1 min of the green flash. Sometimes these motions were complex and lasted for 5–40 s, but ultimately the bead always returned to the centre of the trapping beam. Thereafter, it showed the increased brownian movement characteristic of a free bead (Fig. 2b). We interpreted these complex motions as the result of the bead's being attached to several MTs that depolymerized independently at slightly different times, causing a series of changes in bead position. Because we could not know how many MTs were initially attached to a bead, we focused our analysis on the last motion-inducing event, which resulted from depolymerization of the last bead-associated MT. Bead release was confirmed by moving the stage to assure that the bead remained at the centre of the trap.

In 61 out of 144 experiments, the bead moved slightly away from the centre of the trap before relaxing to the free position (Fig. 2c–e). Because the bead was monitored by the QPD in three dimensions, we could compare the direction of its movements with the orientation of the MT, as observed with differential interference contrast optics. Bead movement was directed towards the minus end in 92% of the

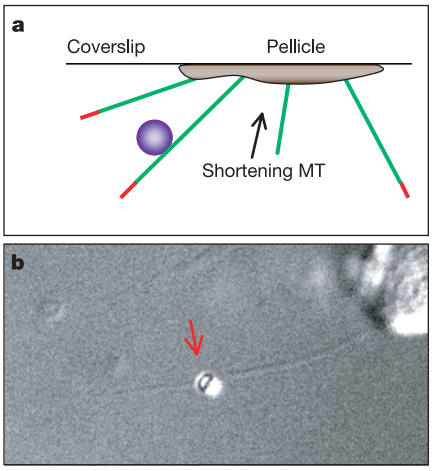

Figure 1 | Experimental design. a, The experimental system (not to scale). Photodamage of the plus-end, rhodamine-conjugated tubulin caps (red) exposes dynamic MTs (green). As the MTs depolymerize, bead motions are measured with laser tweezers. **b**, Differential interference contrast image of a 1-μm bead (arrow) attached to an apparently single MT. Although it is not possible to count the number of MTs attached to each bead at the beginning of an experiment, the narrowness of the histogram of the force magnitudes that developed (Fig. 3a) suggests that almost all of our observations derive from pulls generated by single MTs.

[1]MCD Biology Department, University of Colorado at Boulder, Colorado 80309-0347, USA. [2]Institute of General Pathology and Pathophysiology, Moscow 125315, Russia. [3]National Research Centre for Haematology, Moscow 125167, Russia. [4]Physics Department, Moscow State University, Moscow 119992, Russia. [5]Institute of Theoretical and Experimental Biophysics, Pushchino 142292, Russia.

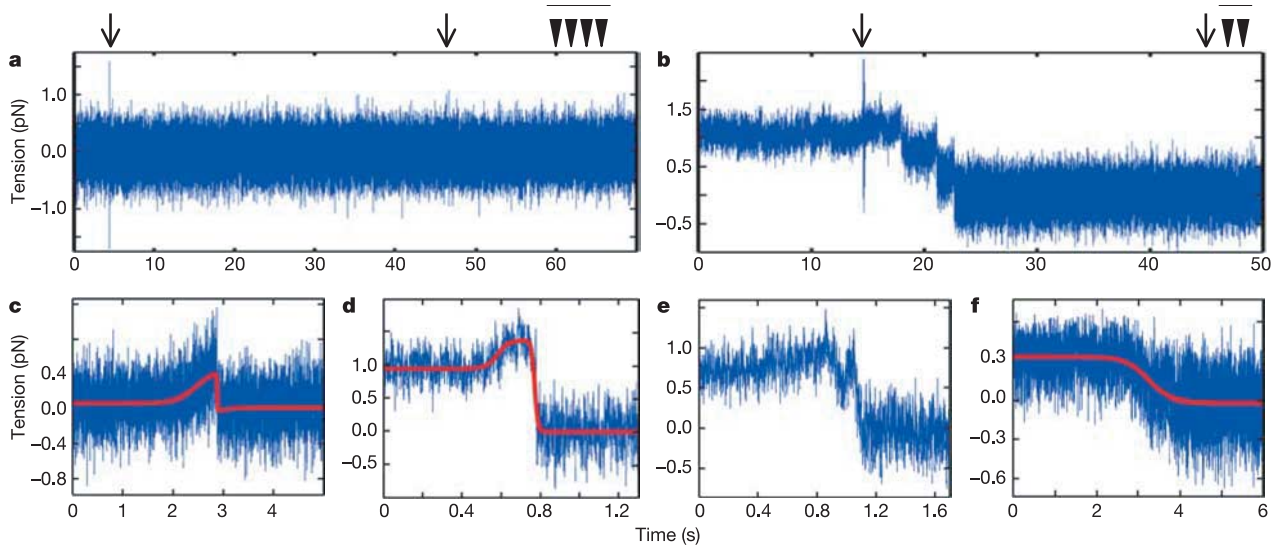

Figure 2 | Example signals. Unprocessed QPD data show changes in bead position and thus force versus time. **a**, A trapped bead not bound to an MT has undergone all routine manipulations: illumination (arrows mark shutter opening and closing) and stage movements (arrowheads). Only brownian motion is seen. **b**, Brownian movement of an MT-associated bead under tension is reduced relative to that in **a**. Low frequency changes before illumination are from tiny drifts of the stage or pellicle. Thereafter, several changes in bead position are distinguished before detachment. **c**–**f**, Examples of final events. Red line shows the curve that was fit to the data with equations (1) and (2) in the Supplementary Information. **c**, **d**, Typical force signals. **e**, A rare force signal superimposed on relaxation. **f**, No force signal and only slow relaxation.

experiments, and force in the orthogonal direction was usually <20% of the paraxial force. Similar experiments were conducted with beads pre-incubated with MT-associated proteins (MAPs) enriched for Tau and microtubule-associated protein 2. These proteins provided a different static MT attachment, but the beads showed depolymerization-dependent, minus-end-directed movements with a frequency comparable to that seen with biotin–streptavidin (in 10 out of 32 trials). Thus, a disassembling MT plus end can develop a pulse of force on beads attached by two distinct static links.

A histogram of force magnitudes (Fig. 3a) shows a mean value of 0.24 ± 0.02 pN ($\pm$s.e.m.; $n = 54$). The force that developed was unaffected by the addition of 2 μM soluble biotin before the initiation of MT depolymerization: beads were not competed from the MTs, the frequency of force-producing events was unchanged, and the forces generated in 15 experiments had the same mean as those without added biotin ($P > 0.05$, Student's t-test). When MAPs were used to couple beads to the MTs, the mean force exerted was 0.22 ± 0.04 pN, which, within experimental error, is equal to the value obtained with biotin–streptavidin coupling. Force magnitudes were independent of both bead–pellicle distance and applied tension (data not shown). The amplitude distribution drops to almost zero at ~0.46 pN, suggesting that this is approximately the maximal force that this system can develop.

Consideration of bead curvature and MT geometry suggests that only 1–2 PFs can attach to a bead simultaneously; thus, bead movement must result from the bending of these linear tubulin arrays. Moreover, the radius of the trapped bead was 500 nm, but the segment of MT that exerted force on the bead was much smaller, probably 20–60 nm (see Supplementary Information). The measured force was thus reduced by a lever arm that is the ratio of these distances (~10). The force at the surface of the bead was therefore ~5 pN, which is about the same as that developed by a single MT-dependent motor enzyme[20]. If a depolymerizing MT end were tracked by a well-designed coupling device, such as an encircling ring that could move freely on the surface of the polymer[21], one would expect all the PFs to act in concert, increasing the depolymerization-dependent force to at least 30–65 pN.

We interpret these observations by a model in which MT depolymerization is triggered distal to the bead, and a wave of disassembly, mediated by outward-curving PFs, propagates towards the minus end of the MT. When the wave reaches the bead and the attached PFs bend out from the MT axis, they exert a brief force on the trapped bead. Such a force should grow in amplitude as the PFs continue bending away from the straight MT surface, while breaking the lateral interactions that constrain the shape of GDP-bound tubulin[10]. Indeed, the maximal observed force was always achieved gradually (Fig. 2c, d). A histogram of the duration of PF bending under load (Fig. 3b) has a broad distribution ranging from 0.03 to 9.5 s, which is likely to reflect, in part, the natural variability in rates of MT depolymerization[22,23]. We tested this supposition by comparing the duration of observed force transient for MTs whose depolymerization rates were varied by altering the concentration of Mg^{2+} ions. Lower Mg^{2+} concentrations, which decrease the rate of MT depolymerization[23], produce longer force transients (Fig. 3c, filled bars). At physiological concentrations of Mg^{2+}(1–4 mM), the duration of force signal and the estimated number of dimers involved suggest that PFs bend under load at a rate of 8–12 dimers s^{-1} (see Supplementary Information). Free MT plus ends, by contrast, depolymerize at ~65 dimers per s per PF[22–25]. The 5–8-fold lower value in our experiments is probably due to both the tension from the trap, which antagonizes PF bending, and the interference provided by tubulin binding to the surface of the bead. Analogous effects may wel explain the decreased depolymerization rate of kinetochore-associated MT[1,26].

No force signal was observed in ~45% of our experiments ($n = 77$); the bead simply moved unidirectionally to the centre of the trap (Fig. 2f). The speed of the bead during this relaxation was variable (Fig. 3). Occasionally it moved as though it were completely free (<20 ms to equilibrium), but ~92% of the events took longer. Relaxations preceded by force production were generally quicker than those without developed force (Fig. 3d). The same trend was seen for relaxation time and force amplitude: smaller forces were commonly followed by slower relaxations (Fig. 3e). These observations suggest that force production by an asymmetric coupler might be impeded by the same processes that slow bead relaxation.

We propose that the variabilities in force generation and bead relaxation times derive from the stochastic peeling of individual PFs

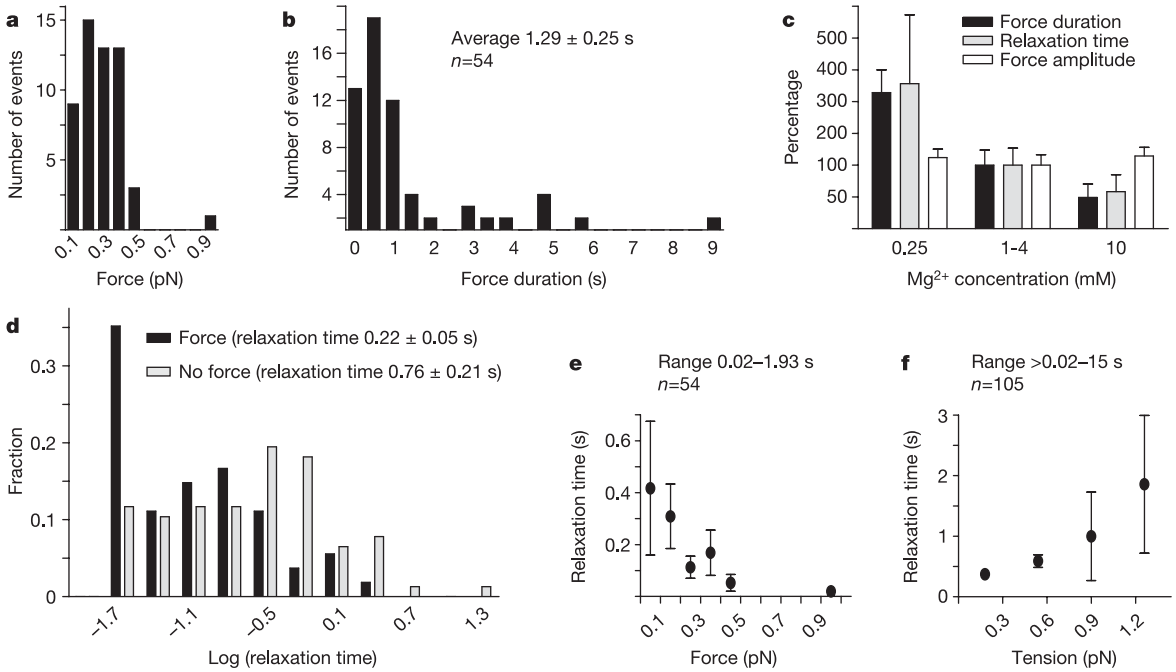

Figure 3 | Analysis of force production. **a**, Histogram of force amplitudes determined from the differences between applied and peak tensions. **b**, Histogram of force duration (that is, the time from the onset of signal increase to the onset of signal decrease). **c**, Force characteristics at different Mg^{2+} concentrations relative to those in physiological conditions (1–4 mM). Both force duration and relaxation time are longer for more slowly depolymerizing MTs. The force amplitudes remain unchanged, however, which suggests that Mg^{2+} ions do not alter the strength of longitudinal bending forces between dimers. **d**, Histogram of the log of relaxation time (that is, the time required for the signal to decrease from maximum to the free bead value). The ordinate shows the fraction of all experiments in each category. **e**, Relaxation time versus force amplitude in the same signal. **f**, Average relaxation time versus applied tension for slow events (>20 ms). Larger error bars at higher tension result from a smaller number of measurements in this tension range. Error bars represent the s.e.m. with 95% confidence intervals (**c**, **e**, **f**).

(Fig. 4). As lateral bonds between PFs separate, the trapped bead will move differently, depending on which PFs relative to the site of bead attachment are the first to split away from their neighbours and peel outward (see Supplementary Information). For example, the bead-associated PFs could peel away slightly before or simultaneously with the peeling of all other PFs (Fig. 4b); this scenario should generate the strongest force. Alternatively, other PFs might peel before those bound to the bead (Fig. 4c); here, the rigidity of the MT segment downstream from the bead would decrease, and the bead should respond to the applied tension by moving closer to the centre of the trap before the appearance of any force transient generated by the curling of bead-attached PFs. Occasionally force might be generated even while the bead is moving towards the centre of the trap (Fig. 2e). More frequently, however, the superposition of these competing processes would probably cancel the force signal altogether. Thus, force production by the asymmetric coupler might be stochastically attenuated owing to asynchrony in PF splitting.

The slow bead relaxations are striking because they imply that the bead retains its attachment to a partially disassembled MT for up to several seconds. Even within 1 s, splitting of the PFs should progress through 8–65 dimers. Throughout this time, however, the bead is not free; thus, longitudinal bonds between dimers beyond the bead must persist, even if some lateral bonds are lost. (If the longitudinal bonds broke, then the bead would jump to the centre of the trap in <20 ms.) We considered whether increased tension on these PFs might facilitate bond breakage; however, slow relaxation times were frequently associated with stronger, not weaker, applied tensions (Fig. 3f). Thus, the duration of bead attachment to a partially disassembled MT can be enhanced by tension that opposes PF bending.

These force-producing events constitute a 'single-shot' mechanism that is mediated by inert, asymmetric couplers. To generate processive movements in association with tubulin depolymerization, there must be a coupling that maintains attachment to the MT

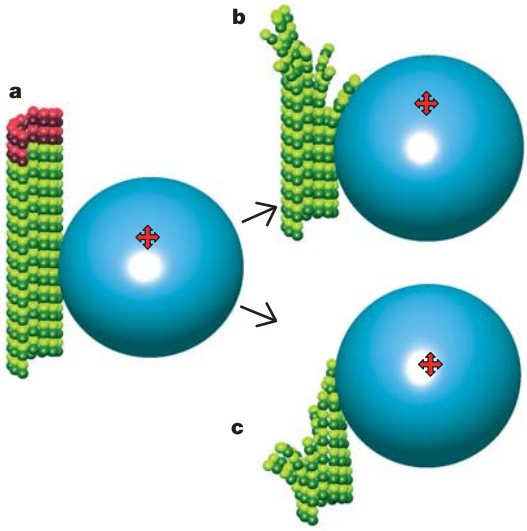

Figure 4 | Models of force production. MT is attached to a bead, which is shown ten times too small. α-Tubulin and β-tubulin are coloured dark and light green, respectively. The red cross marks the trap centre (not shown to scale). **a**, Capped MT with a bead under tension. The bead is attached by roughly three dimers per two adjacent PFs. Red indicates the rhodamine-labelled GMPCPP cap, which was longer and further from the bead than shown. **b**, In scenario 1, the bead-attached PFs peel at the same time or sooner than others. As they curl, the bead is pushed from the trap centre, producing maximal force. **c**, In scenario 2, the bead-attached PFs peel after others, which leaves the bead hanging onto adherent PFs of various lengths. This structure is not rigid and, as it changes owing to continuing disassembly, the tension applied causes the bead to move slowly to the centre of the trap (see Supplementary Information).

surface as the dimers dissociate. Motor enzymes can provide this function[7,8]. The rings formed by the DAM complexes that bind to yeast kinetochores could also contribute to processive movements[21,27]. One of the traits of such couplings in mitosis is that MTs stay attached to kinetochores even when tension is high, and increased tension can induce kinetochore MTs to switch into a polymerization state[28]. We previously proposed that this may occur through rescue of PF bending by constraining properties of the coupler[29]. Our results now suggest a specific molecular mechanism: opposing tension slows PF bending, which in turn inhibits dimer disassembly downstream from the coupler. *In vivo* this process might promote kinetochore MT rescue and contribute to the accuracy of chromosome segregation without requiring any tension-sensing, regulatory enzymes.

METHODS

Instruments and data acquisition. All observations were made on a Zeiss Axiophot2 adapted for laser tweezers as described[30] and modified by the addition of a tracking laser[19]. We sampled the QPD at 4 kHz, the smallest detectable bead displacement was ~5 nm, the smallest force measured was ~0.03 pN, and the free bead relaxation time was <20 ms. At the end of each experiment, the QPD and trap stiffness were calibrated with the same bead by using an acousto-optical deflector (IntraAction) and the equipartition method[19]. Programs for calibration and instrument control were written in LabVIEW 6i (National Instruments). Specimen temperature was regulated to 32.0 ± 0.5 °C by home-made stage and objective lens (Bioptechs) heaters. Samples were maintained in custom-built chambers made from microscope slides that were etched to a depth of ~40 μm over an area just smaller than the coverslip, which was affixed by double-stick tape. The volume of the resulting chamber was 15–20 μl. Solution exchange was driven by a PicoPlus pump (Harvard Apparatus) with thin polyethylene tubes and a valve controller (Warner Instruments).

Reagents and experimental conditions. Tubulin was purified from cow brain by thermal cycling and chromatography, and then labelled with rhodamine or biotin[26]. Pellicles were prepared from *Tetrahymena* and affixed to glass coverslips[6]. Glass microspheres (Polysciences) were coated further with streptavidin conjugated to bovine serum albumin[26] or with MT-associated proteins prepared by boiling the brain proteins that eluted in high salt buffer from the phosphocellulose column used for tubulin purification. Labile MTs were grown from biotinylated and native tubulin (ratio 1:5 to 1:10, total concentration ~1.3 mg ml^{-1}) in 80 mM PIPES buffer (pH 6.9), 1 mM EGTA, 1–4 mM $MgCl_2$ and 2 mM dithiothreitol, 0.2–0.5 mg ml^{-1} of casein and 1 mM GTP. MT growth from pellicles was confirmed by differential interference contrast imaging with a CCD Cascade camera (Roper Scientific). When the MTs were ~15–20 μm, we washed in (at a rate of 30 μl min^{-1}) about three chamber volumes of a mixture of rhodamine-labelled and native tubulin (ratio 1:3, total concentration 0.4 mg ml^{-1}) with 1 mM GMPCPP (Jena Bioscience); this formed MT 'caps' of 1–4 μm. Immediately thereafter, the chamber was washed for 10 min with ten volumes of isothermal buffer containing neither tubulin nor nucleotides. In some experiments, we grew long biotinylated MTs, slowly washed in three chamber volumes of a 1.4 mg ml^{-1} mixture of 1:3 rhodamine-labelled and native tubulin in 1 mM GTP without biotin, and then immediately capped the MTs with unlabelled GMPCPP tubulin. This created MTs that looked in Rhodamine channel like those made by the first method, but which fell apart noticeably faster on illumination. Similar results were obtained with both methods, indicating that the exact position and composition of the photosensitive MT segment were unimportant.

Beads were introduced by flow. The chamber was then inverted for 2–3 min to facilitate binding of the beads to biotinylated MT segments. The chamber was returned to its upright orientation and washed briefly. Beads that remained but failed to associate with MTs settled to the bottom of the chamber. Experiments that used beads covered with MT-associated protein were identical, except that no biotinylated tubulin was used. For experiments in different Mg^{2+} concentrations we grew MTs as above, except that *Chlamydomonas* axonemes (a gift from M. Porter, University of Minnesota) were used for nucleation. After the chamber had been washed with the buffer described above, we exchanged it with a buffer that was identical except for different concentrations of $MgCl_2$. Figure 3c shows result from 16–19 force measurements for each indicated Mg^{2+} concentration (a total of 30–43 observations in each group). Measurements at 1 and 4 mM Mg^{2+} produced statistically indistinguishable results and thus were grouped.

Depolymerization of MTs was induced with the microscope's epi-illumination system, which directed light that stimulated rhodamine fluorescence onto one portion of the pellicle under observation. The average distance from a trapped bead to the edge of the pellicle was 3.8 ± 0.2 μm, which is significantly less than a typical MT; thus, our observations are unlikely to have been affected by the transient presence of the rhodamine-labelled segment. Moreover, in several experiments the MT-associated bead detached before the green light was turned on (as the GMPCPP cap is not perfectly stable). Results from these events were not detectably different, suggesting that the illumination regimen did not create artefacts.

Criteria for choosing beads for study. Normally the trapped bead showed brownian movements, the amplitude of which depended on the stiffness of the trap (Fig. 2a). In nine experiments selected at random, the average trap stiffness was 0.0083 pN nm^{-1} in the plane perpendicular to the optic axis; the average amplitude of brownian motion for a bead in this trap was 23.2 ± 2.1 nm (for a frequency range of 0.1–100 s^{-1}). Binding to MTs longer than ~2 μm did not alter these values detectably. To simplify data analysis we selected beads attached to MTs that were oriented roughly along one of the QPD axes. We routinely tested the attachments by moving the piezo nanopositioning stage (Physic Instrumente) in 0.05-μm steps both parallel and perpendicular to the MT axis. A properly attached bead was displaced from the trap's centre only with movements parallel to the MT. Such tension decreased the amplitude of the bead's movement, but only in the direction parallel to the MT (55 ± 12% per 1 pN of tension; Fig. 2b). Beads that behaved differently from the above were not included in case they were attached to several MTs with different orientations.

Received 5 May; accepted 8 August 2005.

1. Inoue, S. & Salmon, E. D. Force generation by microtubule assembly/disassembly in mitosis and related movements. *Mol. Biol. Cell* **6,** 1619–1640 (1995).
2. Dogterom, M., Kerssemakers, J. W., Romet-Lemonne, G. & Janson, M. E. Force generation by dynamic microtubules. *Curr. Opin. Cell Biol.* **17,** 67–74 (2005).
3. Waterman-Storer, C. M. & Salmon, E. D. Endoplasmic reticulum membrane tubules are distributed by microtubules in living cells using three distinct mechanisms. *Curr. Biol.* **8,** 798–806 (1998).
4. Waterman-Storer, C. M., Worthylake, R. A., Liu, B. P., Burridge, K. & Salmon, E. D. Microtubule growth activates Rac1 to promote lamellipodial protrusion in fibroblasts. *Nature Cell Biol.* **1,** 45–50 (1999).
5. Koshland, D. E., Mitchison, T. J. & Kirschner, M. W. Polewards chromosome movement driven by microtubule depolymerization *in vitro*. *Nature* **331,** 499–504 (1988).
6. Coue, M., Lombillo, V. A. & McIntosh, J. R. Microtubule depolymerization promotes particle and chromosome movement *in vitro*. *J. Cell Biol.* **112,** 1165–1175 (1991).
7. Lombillo, V. A., Nislow, C., Yen, T. J., Gelfand, V. I. & McIntosh, J. R. Antibodies to the kinesin motor domain and CENP-E inhibit microtubule depolymerization-dependent motion of chromosomes *in vitro*. *J. Cell Biol.* **128,** 107–115 (1995).
8. Lombillo, V. A., Stewart, R. J. & McIntosh, J. R. Minus-end-directed motion of kinesin-coated microspheres driven by microtubule depolymerization. *Nature* **373,** 161–164 (1995).
9. Molodtsov, M. I. *et al.* A molecular-mechanical model of the microtubule. *Biophys. J.* **88,** 3167–3179 (2005).
10. Molodtsov, M. I., Grishchuk, E. L., Efremov, A. K., McIntosh, J. R. & Ataullakhanov, F. I. Force production by depolymerizing microtubules: a theoretical study. *Proc. Natl Acad. Sci. USA* **102,** 4353–4358 (2005).
11. Muller-Reichert, T., Chretien, D., Severin, F. & Hyman, A. A. Structural changes at microtubule ends accompanying GTP hydrolysis: information from a slowly hydrolyzable analogue of GTP, guanylyl (α,β)methylenediphosphonate. *Proc. Natl Acad. Sci. USA* **95,** 3661–3666 (1998).
12. Gigant, B. *et al.* The 4 Å X-ray structure of a tubulin:stathmin-like domain complex. *Cell* **102,** 809–816 (2000).
13. Caplow, M., Ruhlen, R. L. & Shanks, J. The free energy for hydrolysis of a microtubule-bound nucleotide triphosphate is near zero: all of the free energy for hydrolysis is stored in the microtubule lattice. *J. Cell Biol.* **127,** 779–788 (1994).
14. Howard, J. & Hyman, A. A. Dynamics and mechanics of the microtubule plus end. *Nature* **422,** 753–758 (2003).
15. Mandelkow, E. M., Mandelkow, E. & Milligan, R. A. Microtubule dynamics and microtubule caps: a time-resolved cryo-electron microscopy study. *J. Cell Biol.* **114,** 977–991 (1991).
16. Hyman, A. A., Salser, S., Drechsel, D. N., Unwin, N. & Mitchison, T. J. Role of GTP hydrolysis in microtubule dynamics: information from a slowly hydrolyzable analogue, GMPCPP. *Mol. Biol. Cell* **3,** 1155–1167 (1992).
17. Vigers, G. P., Coue, M. & McIntosh, J. R. Fluorescent microtubules break up under illumination. *J. Cell Biol.* **107,** 1011–1024 (1988).
18. Allersma, M. W., Gittes, F., deCastro, M. J., Stewart, R. J. & Schmidt, C. F. Two-dimensional tracking of ncd motility by back focal plane interferometry. *Biophys. J.* **74,** 1074–1085 (1998).
19. Visscher, K. & Block, S. M. Versatile optical traps with feedback control. *Methods Enzymol.* **298,** 460–489 (1998).

20. Svoboda, K. & Block, S. M. Force and velocity measured for single kinesin molecules. *Cell* **77,** 773–784 (1994).
21. Westermann, S. *et al.* Formation of a dynamic kinetochore-microtubule interface through assembly of the Dam1 ring complex. *Mol. Cell* **17,** 277–290 (2005).
22. Gildersleeve, R. F., Cross, A. R., Cullen, K. E., Fagen, A. P. & Williams, R. C. Jr Microtubules grow and shorten at intrinsically variable rates. *J. Biol. Chem.* **267,** 7995–8006 (1992).
23. O'Brien, E. T., Salmon, E. D., Walker, R. A. & Erickson, H. P. Effects of magnesium on the dynamic instability of individual microtubules. *Biochemistry* **29,** 6648–6656 (1990).
24. Walker, R. A. *et al.* Dynamic instability of individual microtubules analyzed by video light microscopy: rate constants and transition frequencies. *J. Cell Biol.* **107,** 1437–1448 (1988).
25. Fygenson, D. K., Braun, E. & Libchaber, A. Phase diagram of microtubules. *Phys. Rev. E* **50,** 1579–1588 (1994).
26. Hunt, A. J. & McIntosh, J. R. The dynamic behaviour of individual microtubules associated with chromosomes *in vitro*. *Mol. Biol. Cell* **9,** 249–261 (1998).
27. Miranda, J. L., De Wulf, P., Sorger, P. & Harrison, S. C. The yeast DASH complex forms closed rings on microtubules. *Nature Struct. Mol. Biol.* **12,** 138–143 (2005).
28. Nicklas, R. B. How cells get the right chromosomes. *Science* **275,** 632–637 (1997).
29. McIntosh, J. R., Grishchuk, E. L. & West, R. R. Chromosome–microtubule interactions during mitosis. *Annu. Rev. Cell. Dev. Biol.* **18,** 193–219 (2002).
30. Brouhard, G. J., Schek, H. T. III & Hunt, A. J. Advanced optical tweezers for the study of cellular and molecular biomechanics. *IEEE Trans. Biomed. Eng.* **50,** 121–125 (2003).

Supplementary Information is linked to the online version of the paper at www.nature.com/nature.

Acknowledgements We thank A. Hunt and G. J. Bouchard for sharing the plans for their laser tweezers; T. Perkins for advice, the quadrant photo detector design and programs to help with instrument calibration; H. Higuchi for tips on buffers; and members of McIntosh laboratory, and A. I. Vorobjev and G. P. Georgiev for help and support. V. Sarbash, T. Buxkemper and C. Bowen helped with building the trap. This work was supported in part by grants from the NIH to J.R.M., who is a Research Professor of the American Cancer Society.

Author Information Reprints and permissions information is available at npg.nature.com/reprintsandpermissions. The authors declare no competing financial interests. Correspondence and requests for materials should be addressed to R.M. (richard.mcintosh@colorado.edu).